UDK 67.017:620.3:669.1
Original scientific article/Izvirni znanstveni članek

ISSN 1580-2949
MTAEC9, 52(4)493(2018)

EFFECT OF Y_2O_3 AND ZrO_2 ON THE MICROSTRUCTURE AND MECHANICAL PROPERTIES OF NANO-ODS 21Cr-9Mn-6Ni STEELS

VPLIV Y_2O_3 IN ZrO_2 NA MIKROSTRUKTURO IN MEHANSKE LASTNOSTI NANO-ODS 21Cr-9Mn-6Ni JEKEL

Paleti Kishore Kumar[1], Nimmagadda Vijaya Sai[2], Alluru Gopala Krishna[3]

[1]Veltech Rangarajan Dr Sagunthala R&D Institute of Science and Technology, Department of Mechanical Engineering, Chennai 600 062, India
[2]V R Siddhartha Engineering College, Department of Mechanical Engineering, Viayawada 520 007, India
[3]University College of Engineering, Department of Mechanical Engineering, Jawaharlal Nehru Technological University, Kakinada 533 003, India
kishore.paleti@gmail.com

Prejem rokopisa – received: 2017-11-25; sprejem za objavo – accepted for publication: 2018-02-15

doi:10.17222/mit.2017.199

In this article, nano-oxide dispersion-strengthened (ODS) 21Cr-9Mn-6Ni steels were prepared from elemental powders through vacuum hot pressing. Three ODS steels (21Cr-9Mn-6Ni-0.4Ti-0.3Y_2O_3, 21Cr-9Mn-6Ni-0.4Ti-0.3ZrO_2 and 21Cr-9Mn-6Ni-0.4Ti-0.15Y_2O_3-0.15ZrO_2) were prepared to study the effect of Y_2O_3 and ZrO_2 additions on the microstructure and mechanical properties. The nano-oxide precipitates within the austenite matrix were identified using a transmission-electron microscope equipped with energy-dispersive X-ray spectrometer (TEM-EDX). An addition of Y_2O_3 with ZrO_2 leads to the formation of a bimodal distribution of grains and fine oxide particles of Y-Zr-O and Y-Ti-O in the microstructure of an ODS steel. The results of the tensile test at different temperatures reveal that the strength and elongation of 21Cr-9Mn-6Ni steels are improved with the addition of Y_2O_3 and ZrO_2 due to a stronger interface bonding between large numbers of oxide particles and the austenite matrix.

Keywords: ODS steel, nano-oxide precipitates, tensile strength, elongation, fracture surface

V članku avtorji opisujejo izdelavo z nano-oksidnimi delci disperzijsko utrjenega (ODS) jekla 21Cr-9Mn-6Ni. ODS jeklo je bilo izdelano z vročim stiskanjem iz elementarnih prahov. Tri ODS jekla (21Cr-9Mn-6Ni-0,4Ti-0,3Y_2O_3, 21Cr-9Mn-6Ni-0,4Ti-0,3ZrO_2 in 21Cr-9Mn-6Ni-0,4Ti-0,15Y_2O_3-0,15ZrO_2) so izdelali z namenom, da bi raziskali vpliv dodatkov Y_2O_3 in ZrO_2 na mikrostrukturo in mehanske lastnosti. Nano-oksidne izločke v austenitu so okarakterizirali s presevnim elektronskim mikroskopom, opremljenim z rentgenskim energijskim disperzijskim spektrometrom (TEM-EDX). Ugotovili so, da dodatek Y_2O_3 s ZrO_2 vodi do tvorbe bimodalne porazdelitve kristalnih zrn in drobnih oksidnih delcev Y-Zr-O in Y-Ti-O v mikrostrukturi ODS jekla. Natezni preizkusi pri različnih temperaturah so pokazali, da sta se trdnost in raztezek 21Cr-9Mn-6Ni jekla izboljšala z dodatkom Y_2O_3 in ZrO_2 zaradi močnejše vezi med velikim številom oksidnih delcev in austenitno matrico.

Keywords: ODS jeklo, nano-oksidni izločki, natezna trdnost, raztezek, prelomna površina

1 INTRODUCTION

21Cr-9Mn-6Ni (Nitronic-40) stainless steel is a high-alloyed, high-manganese (Mn) nitrogen (N) strengthened austenitic stainless steel. It has excellent corrosion and oxidation resistance because of a higher amount of chromium (20–30 %) and an increased amount of manganese. Therefore, this steel can be used at elevated temperatures due to its better creep resistance and high-temperature corrosion resistance.[1]

The structural components used in the nuclear industry are subjected to a very high temperature and pressure. Stainless steel of different types, including austenitic steel (AS), martensitic-ferritic steel (M-F/S) and super alloys (nickel based) have good high-temperature properties but poor swelling characteristics.[2] Oxide dispersion strengthened (ODS) steels are the most promising structural materials for nuclear reactors due to many reasons.[3] An ODS steel is manufactured using the dispersion-strengthening mechanism, wherein nano-oxide precipitates are uniformly dispersed in the microstructure.[4]

The superior characteristics of ODS steels depend on the preparation, processing methods[5] and composition design.[6] Y_2O_3 nanoparticles with a cubic structure were used as the oxide particles in the development of ODS steels in recent years.[7] The titanium element was used, along with Y_2O_3, to optimize the nano-particles in the microstructure of ODS steels.[8] Researchers also focused on modifying the microstructure of ODS steels by adding zirconium.[9]

In this paper, the effect of Y_2O_3 and ZrO_2 on the development of the ODS 21Cr-9Mn-6Ni steel was investigated. Also, the microstructure and tensile properties (yield strength, ultimate tensile strength and ductility) of three different ODS steels were studied and compared.

2 EXPERIMENTAL PART

Elemental powders of Fe, Cr, Mn, Ni, Si, Mn_3N_2, Ti and C with a purity of above 99.7 % and a size of 45 μm, delivered from Innomet Powders Pvt. Ltd, India, were used as the starting materials. Different ODS materials such as Y_2O_3 and ZrO_2 powders with a purity of above 99.9 % and a size of 500 nm, from Alfa Aesar, UK, were added to the elemental powders to obtain different ODS steels. The powder blends of three different ODS steel compositions and their designations are listed in **Table 1**.

Table 1: Alloy compositions and designations

S. No.	Composition	Alloy designation
1	Fe-21Cr-9Mn-6Ni-Si-0.15N-0.08C-0.4Ti-0.3Y_2O_3	21-9-6/Y_2O_3
2	Fe-21Cr-9Mn-6Ni-Si-0.15N-0.08C-0.4Ti-0.3ZrO_2	21-9-6/ZrO_2
3	Fe-21Cr-9Mn-6Ni-Si-0.15N-0.08C-0.4Ti-0.15Y_2O_3-0.15ZrO_2	21-9-6/Y_2O_3-ZrO_2

The three ODS steel compositions were properly mixed in a high-energy planetary ball mill (Fristch GmbH, Germany) for 20 h using mechanical alloying (MA). The ball mill operated at 300 min^{-1} and was equipped with a stainless steel vial and balls of a 10-mm diameter. The MA process was conducted at room temperature under an argon protective atmosphere and a ball-to-powder weight ratio of 10:1 maintained in a toluene medium. The as-milled powders were hot pressed (VB ceramics Pvt. Ltd, India) with a pressure of 50 MPa at 1170 °C for 60 min under a vacuum of 10^{-2} torr.

The grain distribution and oxide precipitates were investigated with a high-resolution transmission-electron microscope with energy-dispersive x-ray spectroscopy (HRTEM-EDX) (JEM/2100) operating at 200 kV. Thin-foil specimens of the ODS steel were mechanically thinned to 30 μm and punched into 3-mm discs. Dimpling (GATAN 656) followed by ion milling (GATAN 691) were applied before the TEM studies.

Uni-axial tensile tests were carried out at different temperatures of (301, 573 and 873) K, with a strain rate of 1 mm/min, using a universal testing machine (Instron 1362). The test specimens were machined according to the ASTM-E8 standard, having a gauge length of 15 mm. The fracture-surface morphology of the tensile specimens was characterised using a high-resolution scanning-electron microscope (FEI Quanta FEG 200 HR-SEM).

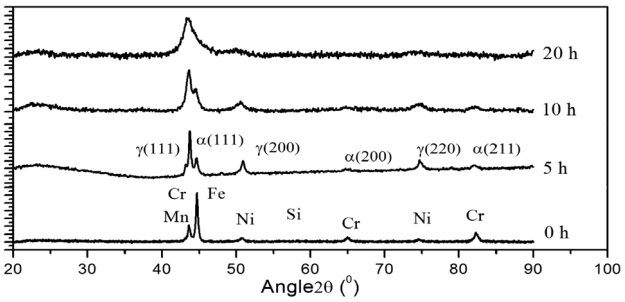

Figure 1: XRD pattern of 21-9-6/Y_2O_3-ZrO_2 powder

3 RESULTS

3.1 Mechanical alloying

The XRD examination of the 21-9-6/Y_2O_3-ZrO_2 elemental composition is represented in **Figure 1**. The elemental composition at 0 h of MA showed individual elemental peaks of Fe, Cr, Mn and Ni. As observed, all the elemental peaks were transformed into a dual-phase structure of austenite (γ) and ferrite (α) phases after 5 h of MA, indicating a dissolution of the elemental powders into the base matrix. After 20 h of milling, the complete structure of the γ phase was observed. The MA process was optimized based on the transition rate between α and γ. The other two ODS compositions also follow similar changes.

3.2 Micro-structural analysis

The density of the three hot-pressed ODS steels was above 95 % of the theoretical density. The TEM microstructures of the 21-9-6/Y_2O_3 and 21-9-6/ZrO_2 steels are shown in **Figures 2a** and **2b**. According to the EDX data, the grains from the figures exhibit an elemental composition (*w*/%) of Fe, Cr, Mn and Ni.

Two different sizes of the grains, namely, a large grain (below 1 μm) and a small grain (below 200 nm) were observed in the bimodal distribution of the grains in the microstructure of the 21-9-6/Y_2O_3-ZrO_2 steel (**Figure 2c**). According to EDX data (**Figure 2d**), the location (+) of smaller grains contains the main elements of Zr, Y, Ti, Si and O.

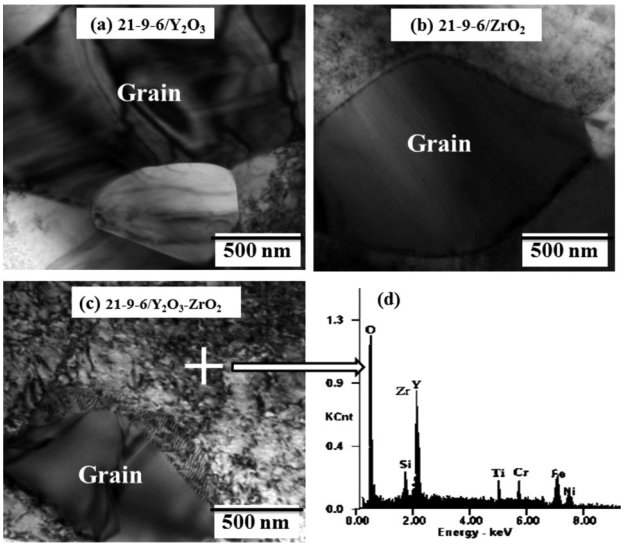

Figure 2: TEM microstructures of ODS steels

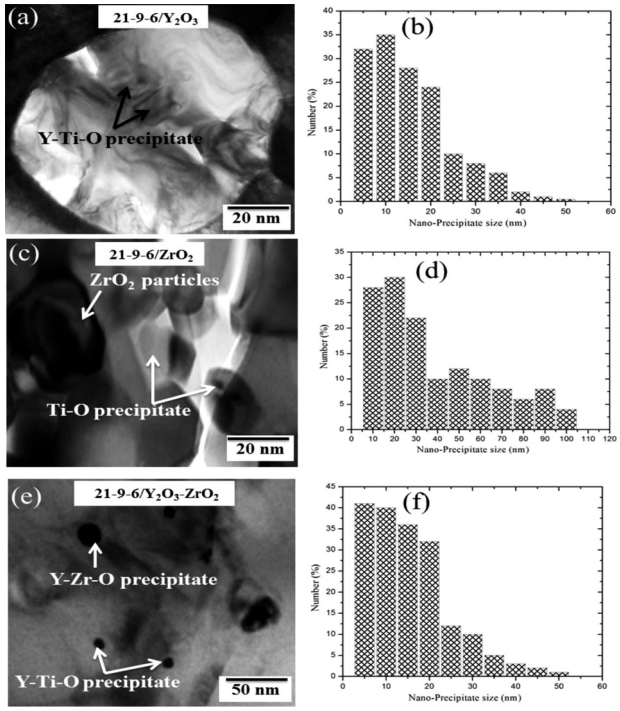

Figure 3: Appearance of nano-oxide precipitates

In order to further study the nano-oxide precipitates, higher-magnification TEM images of the oxide precipitates and size distribution (**Figure 3**) were obtained. The fine oxide precipitates of the Y-Ti-O rich composition of the microstructure of the 21-9-6/Y_2O_3 steel vary from 5 to 50 nm according to the analysis of the particle-size frequency distribution (**Figures 3a** and **3b**). On the other hand, the analysis of the ZrO_2 dispersed ODS steel (21-9-6/ZrO_2) revealed coarse oxide particles of the ZrO_2 composition (**Figure 3c**) and fine precipitates of the Ti-O composition; a large variation in the size of the precipitates can be observed in **Figure 3d**. In the 21-9-6/Y_2O_3-ZrO_2 steel (**Figure 3e**), the precipitates mainly have the Y-Ti-O and Y-Zr-O compositions. The size of most of the oxide particles is in a range of 10–20 nm (**Figure 3f**).

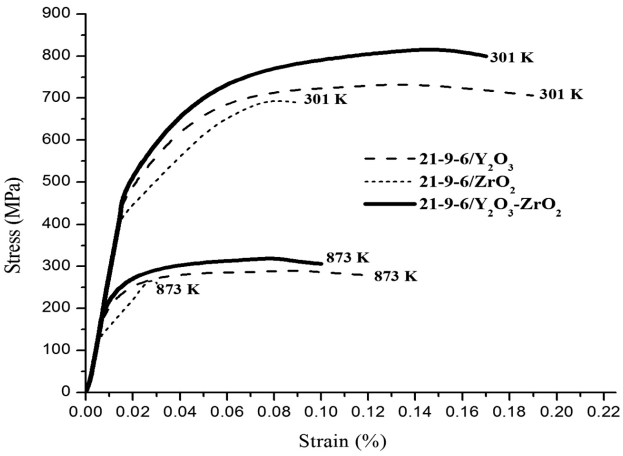

Figure 4: Stress-strain curves for hot-pressed ODS steels

The properties of the nano-oxide precipitates obtained for the three ODS steels are listed in **Table 2**. The calculations were performed on a large data array (a minimum of 1000 nano-sized particles per composition). As it is seen, the 21-9-6/Y_2O_3-ZrO_2 ODS steel exhibited the minimum size and the maximum density of the precipitates.

Table 2: Characteristics of nano-oxide precipitates

ODS steel	Density (per cc)	Size (nm)
21-9-6/Y_2O_3	3.2×10^{15}	14
21-9-6/ZrO_2	0.9×10^{15}	26
21-9-6/Y_2O_3-ZrO_2	5.6×10^{15}	12

3.3 Mechanical properties

3.3.1 Tensile properties

Figure 4 shows the stress-strain curves for three ODS steels at different temperatures. Five replicate tensile tests were performed for each ODS steel at each temperature. The yield strength (YS), tensile strength (UTS) and percent elongation (PE) of the three ODS steels at (301, 573 and 873) K are summarized in **Table 3**. At all the testing temperatures, the 21-9-6/Y_2O_3-ZrO_2 specimen exhibited higher YS and UTS values compared to the other ODS steels, due to the bimodal distribution of powder grains in the microstructure (**Figure 2c**) and

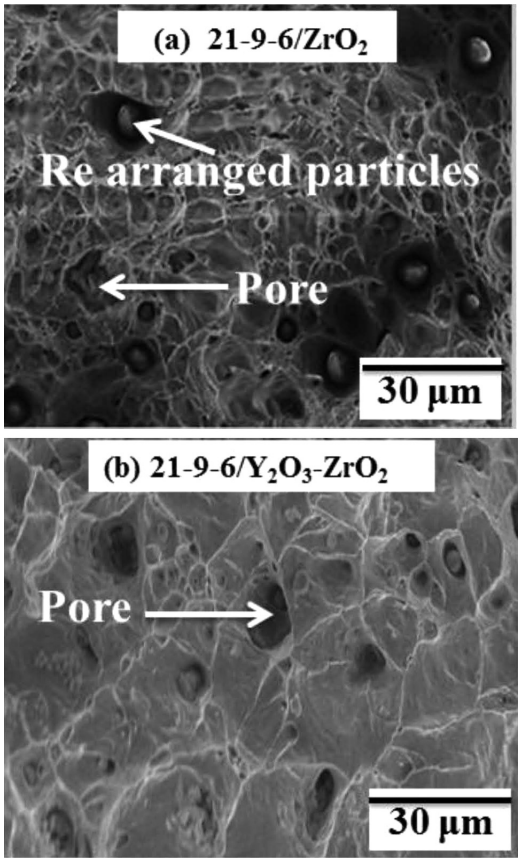

Figure 5: Fracture-surface morphology

Table 3: Mechanical properties of ODS steels at different test temperatures

Composition	301 K			573 K			873 K		
	YS (MPa)	UTS (MPa)	PE (%)	YS (MPa)	UTS (MPa)	PE (%)	YS (MPa)	UTS (MPa)	PE (%)
21-9-6/Y_2O_3	466	734	19	421	667	17	181	291	12
21-9-6/ZrO_2	419	696	9	374	626	6	132	269	3
21-9-6/Y_2O_3-ZrO_2	494	820	17	452	756	15	199	321	10

Table 4: Comparison of microstructures and tensile strengths of different ODS austenitic steels

Composition	Process	Nano-oxide precipitate (nm)	UTS at 301 K (MPa)	UTS at 873 K (MPa)	Ref.
18Cr–8Ni–1Mo–0.5Ti–0.35Y_2O_3	HIP	Y-Ti-Si-O (20)	1000	500	[4]
SS 316 +0.3 Ti + 0.35 Y2O3	HIP	YAH (20)	729	459	[10]
16Cr-13Ni-0.2 Y_2O_3-0.45Zr	HIP+HR	——	970	370	[11]
14Cr-Zr	HIP	Y-Zr-O (8)	994	358	[12]
SS 304+0.35Y_2O_3+0.5Ti	HIP	Y-Ti-O (13)	940	415	[13]
SS 304 +0.3 Ti + 0.35Y_2O_3	HIP	Y-Al-O (20)	1000	–	[14]
21-9-6/Y_2O_3	HP	Y-Ti-O (14)	734	291	Present work
21-9-6/Y_2O_3-ZrO_2	HP	Y-Ti-O & Y-Zr-O (12)	820	321	Present work

also due to the presence of nano-sized Y-Zr-O oxide precipitates (**Figure 3e**), which pinned the dislocations and retarded the grain growth.[9]

However, the PE values for the 21-9-6/Y_2O_3-ZrO_2 steel were slightly reduced when compared to the 21-9-6/Y_2O_3 steel at all the testing temperatures due to the high density of the nano-oxide precipitates (**Table 2**), making the material harder.[10]

3.3.2. Fractographic examination

The fracture surface of 21-9-6/ZrO_2 (**Figure 5a**) contained rearranged particles in some dimples. This indicated that failure occurred only at the particle interface, indicating a brittle failure. Because of this, the specimen exhibited poor mechanical properties (**Table 3**). However, the 21-9-6/Y_2O_3-ZrO_2 steel (**Figure 5b**) clearly showed a ductile fracture evidenced by fine dimples over the entire surface. This was also validated by the tensile properties (**Figure 4** and **Table 3**) of the specimen, showing the highest elongation among the ZrO_2 dispersed ODS steels.

4 DISCUSSION

4.1 Microstructure

The microstructure of the 21Cr-9Mn-6Ni ODS steel was studied based on the additions of different ODS materials (Y_2O_3 and ZrO_2). The microstructure of the Y_2O_3 ODS steel has the appearance of Y-Ti-O nano-oxide precipitates, indicating the presence of Y_2O_3 dissolved in the austenite matrix (**Figure 3a**). It is then combined with Ti to form nano-oxide precipitates of Y–Ti–O in the ODS steel.[8]

The microstructure of the ZrO_2 ODS steel contains ZrO_2 particles (**Figure 3c**) indicating that it does not dissolve in an austenite lattice and may not form a solid solution with Ti. However, in the cases of Y_2O_3 and ZrO_2 added to steel, the ZrO_2 particles are dissolved in the austenite matrix, forming a thermodynamically favourable oxide precipitate with Y_2O_3 (**Figure 3e**). Similar observations[8,11,12] were reported for the behaviour of ZrO_2 during the consolidation of ODS steel.

4.2 Mechanical properties

The mechanical properties of the 21Cr-9Mn-6Ni ODS steel were studied as a function of different ODS materials (Y_2O_3 and ZrO_2) added.

The Y_2O_3 ODS steel from the present work exhibited a lower UTS value (**Table 4**) compared to the other ODS austenitic steels developed previously. This is due to the HIP[4,10,13,14] consolidation process used for developing ODS steels, which is an effective process compared to the HP process used in this study.

The Y_2O_3 and ZrO_2 ODS steels from the present wok can have the tensile-strength values comparable to the other ODS steels developed previously.[10–14] The bimodal distribution of the grains (**Figure 2c**) and the formation of the Y-Ti-O and Y-Zr-O nano-oxide precipitates (**Table 2** and **Figure 3e**) in the microstructure explain the high tensile-strength values of the ODS 21Cr-9Mn-6Ni steel.

5 CONCLUSIONS

In this research, the authors investigated the microstructure and mechanical properties of Y_2O_3 and ZrO_2 21Cr-9Mn-6Ni-0.4Ti ODS steels. Three ODS steels (21-9-6/Y_2O_3, 21-9-6/ZrO_2, 21-9-6/Y_2O_3-ZrO_2) were made from elemental powders and consolidated by hot pressing. The results were compared and the conclusions are summarized as follows:

According to the TEM results, a bimodal distribution of the grains was found in the microstructure of the

21-9-6/Y_2O_3-ZrO_2 ODS steel, which indicates that ZrO_2 was decomposed and dissolved into the austenite matrix only in the presence of Y_2O_3.

The nano-oxide precipitates in the 21-9-6/Y_2O_3-ZrO_2 steel have a smaller size and a higher density compared to the other two ODS steels. This is due to the formation of Y-Zr-O and Y-Ti-O oxide precipitates with the additions of Y_2O_3 and ZrO_2 particles.

The composition of the 21-9-6/Y_2O_3-ZrO_2 ODS steel showed higher yield and tensile strengths compared to the other two ODS steels studied. This is due to the homogeneous dispersion of the nano-oxide particles and bimodal distribution of powder grains.

The fractography studies of the surface of the 21-9-6/Y_2O_3-ZrO_2 ODS steel revealed that the presence of regular-shaped dimples indicates a ductile failure.

Based on the above findings, it can be concluded that an addition of Y_2O_3 and ZrO_2 facilitates attractive mechanical properties of 21-9-6 steels.

Acknowledgements

The authors would like to express their gratitude to Veltech & JNTUK, India, for giving them an opportunity to publish this paper. The TEM study was carried out at the PSG Institute of Advanced Studies (Nanotech Research Lab), India.

6 REFERENCES

[1] J. W. Elmer, G. F. Ellsworth, J. N. Florando, I. V. Golosker, R. P. Mulay, Microstructure and mechanical properties of 21-6-9 stainless steel electron beam welds, Metallurgical and materials transactions A, 48A (**2017**), 1771–1787, doi:10.1007/s11661-017-3996-y

[2] S. Wang, M. Zhang, H. Wu, B. Yang, Study on the dynamic recrystallization model and mechanism of nuclear grade 316LN austenitic stainless steel, Materials characterization, 118 (**2016**), 92–101, doi:10.1016/j.matchar.2016.05.015

[3] C. C. Eiselt, H. Schendzielorz, A. Seubert, B. Hary, D. Cedat, ODS-materials for high temperature applications in advanced nuclear systems, Nuclear Materials and Energy, 9 (**2016**), 22–28, doi:10.1016/j.nme.2016.08.017

[4] Z. Zhou, S. Yang, W. Chen, L. Liao, Y. Xu, Processing and characterization of a hipped oxide dispersion strengthened austenitic steel, Journal of nuclear materials, 428 (**2012**), 31–34, doi:10.1016/j.jnucmat.2011.08.027

[5] P. Kishore Kumar, N. Vijaya Sai, A. Gopala Krishna, Influence of sintering conditions on microstructure and mechanical properties of alloy 218 steels by powder metallurgy route, Arabian journal for science and engineering, (**2017**), doi:10.1007/s13369-017-3015-z

[6] O. Khalaj, B. Masek, H. Jirkova, A. Ronesova, J. Svoboda, Investigation on new creep- and oxidation-resistant materials, Mater. Tehnol., 49 (**2015**) 4, 645–651, doi:10.17222/mit.2014.210

[7] D. Sun, C. Liang, J. Shang, J. Yin, X. Zhang, Effect of Y_2O_3 contents on oxidation resistance at 1150 °C and mechanical properties at room temperature of ODS Ni-20Cr-5Al alloy, Applied Surface Science, 385 (**2016**), 587–596, doi:10.1016/j.apsusc.2016.05.143

[8] C. Lu, Z. Lu, R. Xie, Z. Li, L. Wang, Effect of Y/Ti atomic ratio on microstructure of oxide dispersion strengthened alloys, Materials Characterization, 134 (**2017**), 35–40, doi:10.1016/j.matchar.2017.10.004

[9] A. Mahmutovic, A. Nagode, M. Rimac, D. Mujagic, Modification of the inclusions in austenitic stainless steel by adding tellurium and zirconium, Mater. Tehnol., 51 (**2017**) 3, 523–528, doi:10.17222/mit.2015.297

[10] Y. Miao, K. Mo, Z. Zhou, X. Liu, K. Lan, G. Zhang, M. K. Miller, K. A. Powers, Z. Mei, J. Park, J. Almer, J. F. Stubbins, On the microstructure and strengthening mechanism in oxide dispersion strengthened 316 steel: A coordinated electron microscopy, atom probe tomography and in situ synchrotron tensile investigation, Materials science and engineering A, 639 (**2015**), 585–596, doi:10.1016/j.msea.2015.05.064

[11] T. Graning, M. Rieth, J. Hoffmann, A. Moslang, Production, microstructure and mechanical properties of two different austenitic ODS steels, Journal of nuclear materials, 487 (**2017**), 348–361, doi:10.1016/j.jnucmat.2017.02.034

[12] L. Zhang, L. Yu, Y. Liu, C. Liu, H. Li, J. Wu, Influence of Zr addition on the microstructures and mechanical properties of 14Cr ODS steels, Materials science and engineering A, 695 (**2017**), 66–73, doi:10.1016/j.msea.2017.04.020

[13] M. Wang, Z. Zhou, H. Sun, H. Hu, S. Li, Microstructural observation and tensile properties of ODS-304 austenitic steel, Materials science and engineering A, 559 (**2013**), 287–292, doi:10.1016/j.msea.2012.08.099

[14] Y. Miao, K. Mo, Z. Zhou, X. Liu, K. Lan, G. Zhang, M. K. Miller, K. A. Powers, J. Almer, J. F. Stubbins, In situ synchrotron tensile investigations on the phase responses within an oxide dispersion-strengthened (ODS) 304 steel, Materials science and engineering A, 625 (**2015**), 146–152, doi:10.1016/j.msea.2014.12.017